Selenium-Doped Rh₆ Carbonyl Clusters on MgO: Structures and Promoting Effects In Ethene Hydroformylation

Yasuo Izumi and Yasuhiro Iwasawa*

Department of Chemistry, Faculty of Science, The University of Tokyo, Hongo, Bunkyo-ku, Tokyo 113, Japan
(Received: June 17, 1992; In Final Form: August 17, 1992)

Selenium-modified $Rh_6(CO)_{16}$/MgO catalysts were prepared by the reaction of $Rh_6(CO)_{16}$/MgO with $(CH_3)_2Se$ in order to examine the promoting effect of an electronegative additive on Rh catalysis for ethene hydroformylation. The deposited Se ($Se/Rh_6 = 0.6$) enhanced the rate of propanal formation 1.9 times as compared with the case of an undeposited catalyst. The selectivity of the hydroformylation was improved from 20 to 50% by the Se addition. To the contrary, the monotonous suppression of ethane formation by increasing the Se amount was observed. Further doping of Se reduced the hydroformylation activity. TPD, IR, and Se K-edge and Rh K-edge EXAFS revealed that $(CH_3)_2Se$ reacted with the Rh atoms of partially-decarbonylated Rh_6 species on the MgO surface, forming Se–Rh bonds at a distance of 0.244 nm. XPS data suggested that the oxidation state of Se in the catalyst is Se⁻, while Rh is in a nearly metallic state. CO adsorbs on the rhodium atoms bonded to Se, which is contrasted to blocking of the neighboring Rh sites by Se atom observed with usual impregnated Rh catalysts. The structures of the Se-undoped and -doped Rh_6 clusters on MgO are presented in relation to the active site of the cluster catalyst. The data indicate an advantage of molecular clusters over impregnated particles in adsorption capability and catalysis.

Introduction

Metal clusters have often been used as precursors of supported metal catalysts. The most prevailing advantage for using metal clusters is to prepare dispersed, fine metal particles on inorganic oxides.[1] It is possible to control the molecular size of cluster particles on supports by changing the number of nuclear metal atoms. Kirlin et al. reported the dependency of catalytic activity on cluster sizes for supported rhenium carbonyl clusters (HRe-$(CO)_5$ and $H_3Re_3(CO)_{12}$) on MgO.[2]

Another advantage in using metal clusters is that metal clusters are considered as simulated structures of active particular ensembles like step sites and kink sites on supported metal particles. Better understanding of essential factors of solid catalysis may be obtained in these systems rather than in conventional catalysts. Furthermore, new catalytic sites or ensembles can be created by using metal cluster precursors supported on inorganic oxides. Nevertheless, precursor clusters with well-defined structures are often converted to ill-defined metal particles after treatments or during catalytic reactions, even if they were dispersed as fine particles less than 1.0 nm.

The promoting effect of the second element added on metal catalysts is a subject to examine in metal cluster systems when the structure of the second-element-doped metal cluster is defined on a molecular level. Rhodium is an industrially important element for synthesis gas reaction, hydroformylation, etc., and cationic Rh sites rather than metallic Rh⁰ have been supposed to be active for CO insertion elementary step.[3] In fact, doping of sulfur as an anionic element to Rh or Ni catalysts resulted in the augmentation of selectivity for the formation of oxo compounds.[4,5] Selenium also behaves as an electronegative additive, but the ionic radius is 1.08 times larger than that of sulfur (1.06 times for atomic radius). Se-doped Rh/ZrO_2 or Rh/SiO_2 catalysts prepared from $(CH_3)_2Se$ or SeO_2 showed an increase in selectivity for oxygenates in ethene hydroformylation at an optimum Se/(surface Rh) ratio.[6,7] The examples of the promoting effects by electronegative elements are still much fewer than those by electropositive elements and transition metal elements.

In the present report we studied the structures of Se-undoped and -doped $Rh_6(CO)_{16-x}$ clusters on MgO by EXAFS, FT-IR, TPD, and adsorption. The enhancement of the reaction rate and selectivity of ethene hydroformylation by Se addition was found. The cluster metal framework on MgO was maintained, and $(CH_3)_2Se$ in gas-phase selectively reacted with the partially-decarbonylated Rh_6 clusters on MgO at 398 K to form direct Se–Rh bonds, by which the nearest and next-nearest neighboring Rh sites[8] for the attached Se atom were created.
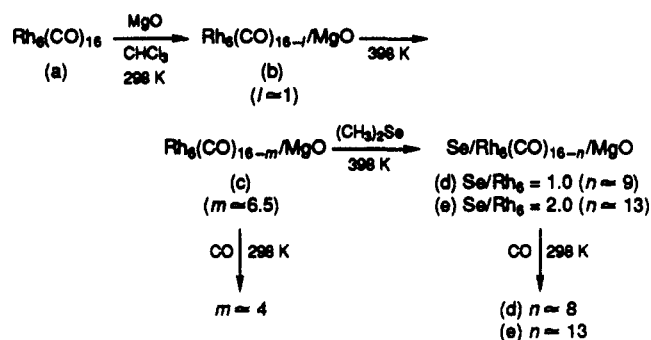
Experimental Section

Se-doped catalysts were prepared by the following procedure (Scheme I). $Rh_6(CO)_{16}$ (0.3 g) (Aldrich Chemical Co.) was dissolved in 500 mL of chloroform which had been purified by reflux over 5A molecular sieves and distillation. MgO (Soekawa, 99.999%) pretreated at 773 K for 2 h in vacuum was immersed with the solution, followed by evacuation to remove the solvent. The Rh loading was chosen in the range 1.3–5.0 wt % as the convenience of each experiment. All procedures of preparation were conducted in a flow of Ar (99.9999%) or under vacuum. $Rh_6(CO)_{16}$/MgO was heated to 398 K under vacuum to remove about one-third of ligand CO. Then the partially-decarbonylated Rh clusters were contacted with the vapor of $(CH_3)_2Se$ at 398 K for 30 min in a closed circulating system connected to a vacuum line. After reaction for 30 min, the system was evacuated for 1 min. In the range of $0 < Se/Rh_6 < 4$, all the $(CH_3)_2Se$ reacted with the MgO-supported clusters because no $(CH_3)_2Se$ remained in the gas phase after reaction for 30 min. $(CH_3)_2Se$ adsorbed physically on the MgO, and the physisorbed $(CH_3)_2Se$ easily desorbed by evacuation at 298 K.

Se K-edge and Rh K-edge EXAFS spectra were measured in a transmission mode at a beam line 10B of the Photon Factory in the National Laboratory for High Energy Physics (Proposal No. 87013). The EXAFS spectra were taken in an EXAFS cell without contacting air by using a transfer technique from the closed circulating system for sample preparation to the cell. The EXAFS analysis was carried out using the theoretical phase shift and amplitude functions, on the basis of the formula of plane-wave single scattering theory,[9] and also the empirical ones extracting from the measurements of Rh foil, $Rh_6(CO)_{16}$, and $(CH_3)_2Se$ as
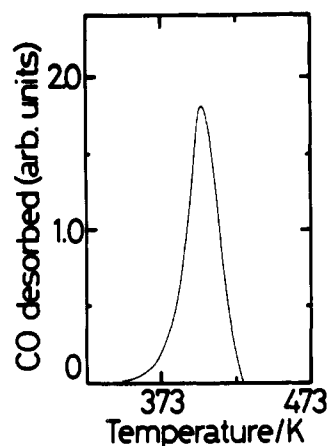
Figure 1. TPD spectrum for Rh$_6$(CO)$_{16}$/MgO.

model compounds for Rh–Rh, Rh–C$_t$, Rh–C$_b$, Rh(–C–)O, and Se–C bonds, respectively. The Fourier transform of the k^3-weighted EXAFS oscillation was carried out over the ranges of 30–140 and 30–150 nm^{-1} for Se and Rh K-edge EXAFS, respectively. The filtering ranges for inverse Fourier transform to k space were 0.16–0.25 and 0.12–0.30 nm for Se and Rh K-edge EXAFS, respectively. In the curve-fitting analysis for Rh K-edge EXAFS, the Debye–Waller factors σ_i for each coordination shell were fixed (=0.005 nm), and the coordination numbers N_i for Rh–Rh, Rh–C$_t$, Rh–C$_b$, and Rh(–C–)O were determined by comparison with the N_i obtained from the analysis of Rh$_6$(CO)$_{16}$ or Rh foil at the same fixed σ_i value. In the case of Se K-edge EXAFS the σ_i's were floated, but the N_i's were not corrected by the amplitude reduction factor S_i because of the lack of model compounds for Se–Rh bonding to estimate the S_i (also for Rh–Se bond in the Rh K-edge EXAFS). The errors in the present analysis for coordination number and bond distance are regarded as 15–20 and 0.5–1.0%, respectively. The degree of the curve fitting to experimental data was estimated by a reliability factor (Rf):

$$Rf = \int |k^3\chi^{obs}(k) - k^3\chi^{calc}(k)|^2\, dk / \int |k^3\chi^{obs}(k)|^2\, dk$$

XPS spectra for Se 3d$_{5/2}$, Rh 3d$_{5/2}$ and 3d$_{3/2}$ were recorded on a Shimadzu ESCA750 spectrometer. The samples were transferred into the XPS chamber by a glovebox technique without contacting air. The binding energy of C 1s was referred to the value of the 4f level (83.8 eV) of deposited Au and the XPS binding energies were normalized by the C 1s energy.

Ethene hydroformylation was carried out at 398 K and 40.0 kPa (C$_2$H$_4$:CO:H$_2$ = 1:1:1) in a closed circulating system (dead volume: 120 cm^3) with a U-shaped liquid N$_2$–acetone trap (179 K). The reaction products were analyzed by a gas chromatograph using a 2-m column of VZ-10 at 353 K for ethene and ethane and a 4-m column of DOS at 353 K for propanal and propanol. Methane was also analyzed by a 2-m column of 5A molecular sieves at 353 K.

IR spectra were measured under in situ reaction conditions by an FT-IR spectrometer (JASCO FTIR7000). MgO (0.03 g) was pressed into a self-supporting disk of 20 mm in diameter which was placed in an IR cell with two NaCl windows which was combined with a closed circulating system. A chloroform solution of Rh$_6$(CO)$_{16}$ was added dropwise to the MgO in Ar (99.9999%) atmosphere. The spectra were recorded by subtracting the gas-phase spectra.

Results

TPD Spectra for Rh$_6$(CO)$_{16}$-Derived Catalysts. The TPD spectrum for Rh$_6$(CO)$_{16}$/MgO in vacuum is shown in Figure 1. The ligand CO desorbed around 400 K, and the desorption was completed until 430 K. About one-third of ligand CO was desorbed before 398 K. No CO$_2$ desorbed. When the Rh$_6$/MgO were reacted with (CH$_3$)$_2$Se at 398 K, 0.9 mol of CO per Rh$_6$-(CO)$_{16}$ were evolved and also three IR peaks (1632, 1524, 1388 cm^{-1}) which can be assigned to formates were observed.

TABLE I: Results of the Curve Fitting Analyses for Se K-Edge EXAFS Spectra of Se-Doped Rh$_6$/MgO[a]

		Se–Rh		
sample	Se/Rh$_6$	N[b]	r/nm	Rf
d	1.0	1.3	0.244	0.043
d[c]	1.0	1.4	0.244	0.047
e	2.0	1.4	0.243	0.050
e[c]	2.0	1.3	0.243	0.037

[a] The notation of the samples is same as in Scheme I. [b] The reduction factor is not considered. [c] After ethene hydroformylation (60 min).

EXAFS Observation for Selenium-Deposited Rh$_6$/MgO Catalysts. The structures of Rh$_6$/MgO and Se-deposited Rh$_6$/MgO catalysts in the preparation processes of catalysts shown in Scheme I were examined by the EXAFS analysis of Se K-edge and Rh K-edge absorption data. We varied the ratio of Se/Rh$_6$ (=0, 1.0, and 2.0).

The Fourier transform of the Se K-edge EXAFS spectrum for the Se-modified Rh$_6$/MgO with Se/Rh$_6$ = 1.0 in Figure 2b showed only one peak around 0.22 nm (phase shift uncorrected). The oscillation in the higher wavenumber region (Figure 2a) suggests the presence of heavy atom scatterers around the Se atom. To analyze the peak around 0.22 nm, the peak was inversely transformed to the k-space oscillation, followed by the curve-fitting analysis in Figure 2c which confirms the peak to be due to the Se–Rh bond. The determined bond distance (r) and coordination number (N) for Se–Rh are shown in Table I. Next, we tried the two-wave fitting (Se–Rh and Se–C) because of the probability that a part of the two methyl ligands of (CH$_3$)$_2$Se might remain, but the Rf was worse than that for one-wave fitting (Se–Rh). These results suggest that (CH$_3$)$_2$Se reacted with the partially-decarbonylated Rh$_6$ cluster at 398 K, releasing the CH$_3$ ligands. The N and r after ethene hydroformylation for 60 min were 1.4 (the reduction factor S_i is not considered) and 0.244 nm, respectively, which were almost the same as those for the catalyst before catalytic reaction (1.3, 0.244 nm) (Table I).

The analysis for the catalyst with Se/Rh$_6$ = 2.0 showed N = 1.4 and r = 0.243 nm. In the case of this catalyst, it was observed that a small amount of acetaldehyde was formed at the initial stage (0–15 min) of ethene hydroformylation at 398 K. In the catalyst with Se/Rh$_6$ = 2.0, a small portion of the methyl ligand bonded to Se may have remained after the reaction of (CH$_3$)$_2$Se with the cluster.

Figures 3 and 4 showed the Rh K-edge EXAFS data for the Se-undoped and Se-doped Rh$_6$/MgO catalysts. On the basis of the analysis for Rh$_6$(CO)$_{16}$ as a model compound, the N_{Rh-Rh} for the catalyst (Se/Rh$_6$ = 2.0) was obtained to be 4.0 (Table II), which implies that the incipient Rh$_6$ framework remained unchanged after the reaction between Rh$_6$/MgO and (CH$_3$)$_2$Se at 398 K.

Catalytic Ethene Hydroformylation. As is shown in Figure 5, ethane (80%), propanal (17%), and propanol (3.3%) were produced on Rh$_6$/MgO without Se in ethene hydroformylation at 398 K. With the increase of deposited Se the activity (the reaction rate per *total* Rh atoms) for propanal increased and reached a maximum around Se/Rh$_6$ = 0.6. The maximum activity was 1.9 times higher than the activity of the Se-undoped catalyst. This is contrasted to a monotonous depression for the formations of ethane and propanol. The selectivity for hydroformylation (propanal and propanol) showed a maximum at Se/Rh$_6$ = 1.0, where the selectivity was 50%. Further doping of Se (Se/Rh$_6$ > 1.0) reduced the rates of both hydroformylation and ethane formation. The decrease in the rate of ethane formation was more drastic.

For the evaluation of unblocked Rh sites after the doping of Se, we observed CO uptake on the Rh$_6$/MgO catalysts with different Se/Rh$_6$ ratios (Figure 6). The amount of CO adsorbed decreased with Se deposition. The sum of this CO uptake and the remaining ligand CO of the Rh cluster after the reaction with (CH$_3$)$_2$Se at 398 K is also shown in Figure 6, which also decreased with an increase of Se.
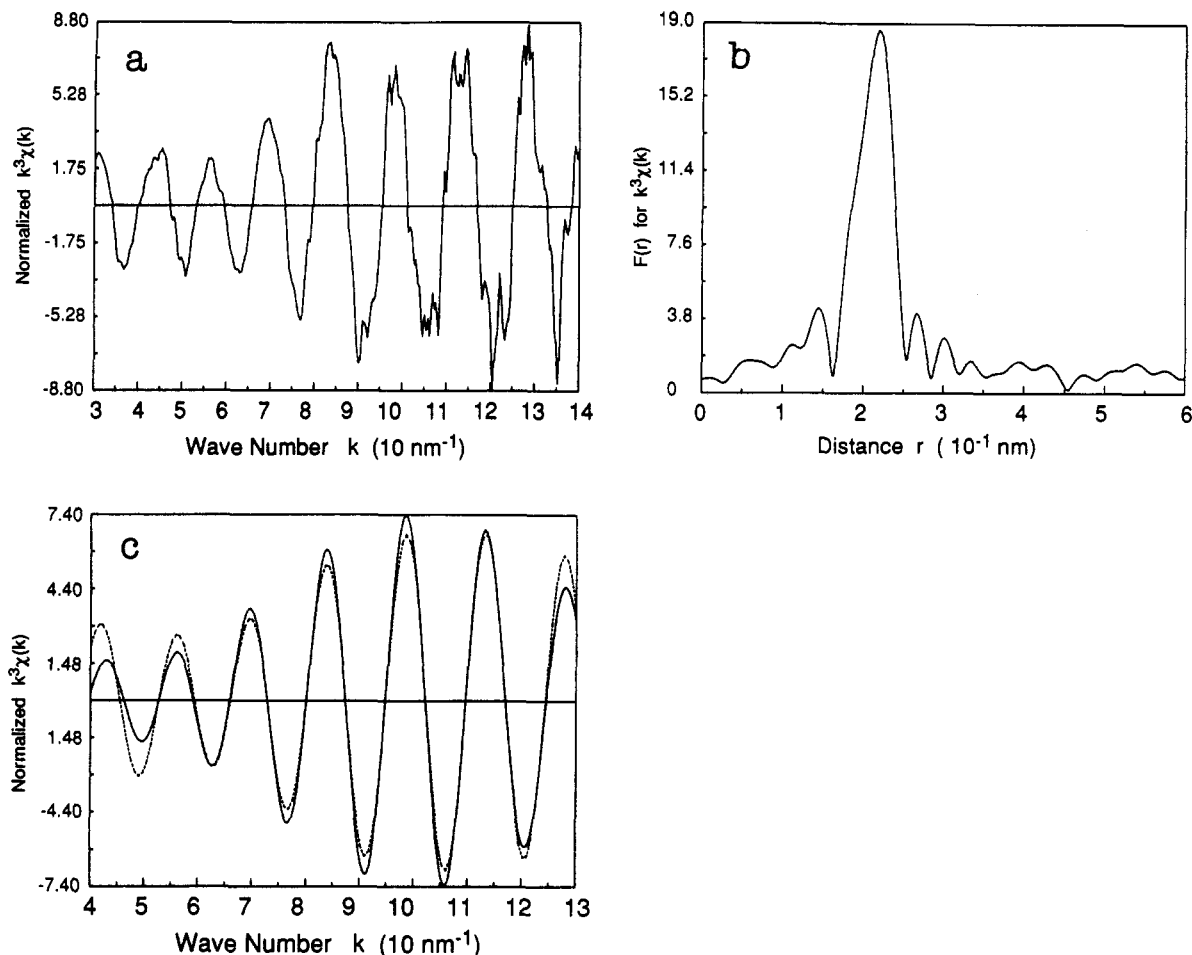
Figure 2. EXAFS spectra for Se K-edge of Se-doped Rh_6/MgO (Se/Rh_6 = 1.0): (a) k^3-weighted EXAFS oscillation, (b) its associated Fourier transform, and (c) inversely Fourier transformed curve-fitting analysis (—, observed; - -, calculated).

TABLE II: Results of the Curve Fitting Analyses for Rh K-Edge EXAFS Spectra of Rh_6/MgO and Se-Doped Rh_6/MgO[a]

		Rh–Rh		Rh–Se		Rh–C_t		Rh–C_b		Rh(–C–)O		
	Se/Rh_6	N	r/nm	N^b	r/nm	N	r/nm	N	r/nm	N	r/nm	Rf
a		(4)	0.277			(2)	0.187	(2)	0.219	(4)	0.306	0.035
b	0	3.8	0.276			1.8	0.185	1.9	0.215	4.0	0.307	0.054
c	0	3.8	0.275			1.3	0.185	1.6	0.219	3.0	0.306	0.034
d	1.0	3.7	0.276	0.4	0.244	1.2	0.187	1.5	0.207	2.4	0.310	0.021
d[c]	1.0	3.9	0.275	0.4	0.244	1.5	0.189	1.7	0.206	3.1	0.310	0.041
e	2.0	4.0	0.273	0.7	0.243	0.9	0.187	1.1	0.207	1.2	0.309	0.017
a[d]		4	0.2776			2	0.1864	2	0.2168	4	0.306[e]	

[a] The notation of the samples is same as in Scheme I. [b] The reduction factor is not considered. [c] After ethene hydroformylation (60 min). [d] Determined by XRD. [e] The average for terminal and bridged CO.

TABLE III: Wavenumbers of IR Peaks for $Rh_6(CO)_{16}$, Rh_6/MgO, and Se-Doped Rh_6/MgO

substance	wavenumber/cm^{-1}	
	twin, terminal	bridged
$Rh_6(CO)_{16}$[a]	2105 w, 2070 s, 2047 w, 2040 w, 2022 mw, 2020 mw	1833 w, 1793 s
Rh_6/MgO (298 K)	2090 w (sh), 2071 s, 2055 m, 2046 w, 2027 w, 2022 m	1800 s
Rh_6/MgO (398 K)	2091 s, 2072 s, 2055 w, 2046 vw, 2022 m	1800 s
Se/Rh_6/MeO (Se/Rh_6 = 1.0)	2092 m, 2067 s, 2055 m, 2046 vw, 2022 m	1800 s
Se/Rh_6/MgO (Se/Rh_6 = 2.0)	2094 s, 2047 w, 2023 s	1805 m

[a] In ref 10.

FT-IR Observation for Selenium-Deposited Rh_6/MgO. Figure 7b shows the spectrum for the incipient Rh_6/MgO. For comparison the peaks for $Rh_6(CO)_{16}$ in nujol are also shown in Table III.[10] After the sample was heated at 398 K in vacuum, the IR

TABLE IV: Wavenumbers of IR Peaks for Rh_6/MgO and Se-Doped Rh_6/MgO in Ethene Hydroformylation

substance	wavenumber/cm^{-1}	
	twin, terminal	bridged
Rh_6/MgO	2092 w (sh), 2071 s, 2055 w, 2046 vw, 2021 s	1802 s
Se/Rh_6/MgO (Se/Rh_6 = 1.0)	2094 s, 2071 w (sh), 2055 w, 2046 vw, 2022 s	1797 s

peaks were not significantly changed, though their intensities reduced (Figure 7c). The spectrum in Figure 8a shows the IR spectrum for the Se-deposited Rh_6/MgO (Se/Rh_6 = 1.0) after the reaction of the supported cluster with $(CH_3)_2Se$ at 398 K. Further CO ligands desorbed upon Se deposition, but the peak pattern was similar to those for Rh_6/MgO (298 K) and Rh_6/MgO (398 K), as shown in Figure 7b or c and Table III. For the catalyst with Se/Rh_6 = 2.0 the twin CO peaks at 2094 and 2023 cm^{-1} and a broad bridge-CO peak at 1805 cm^{-1} were observed (Table III).

In situ IR spectra in ethene hydroformylation on Se-undoped Rh_6/MgO and Se/Rh_6/MgO with Se/Rh_6 = 1.0 are shown in
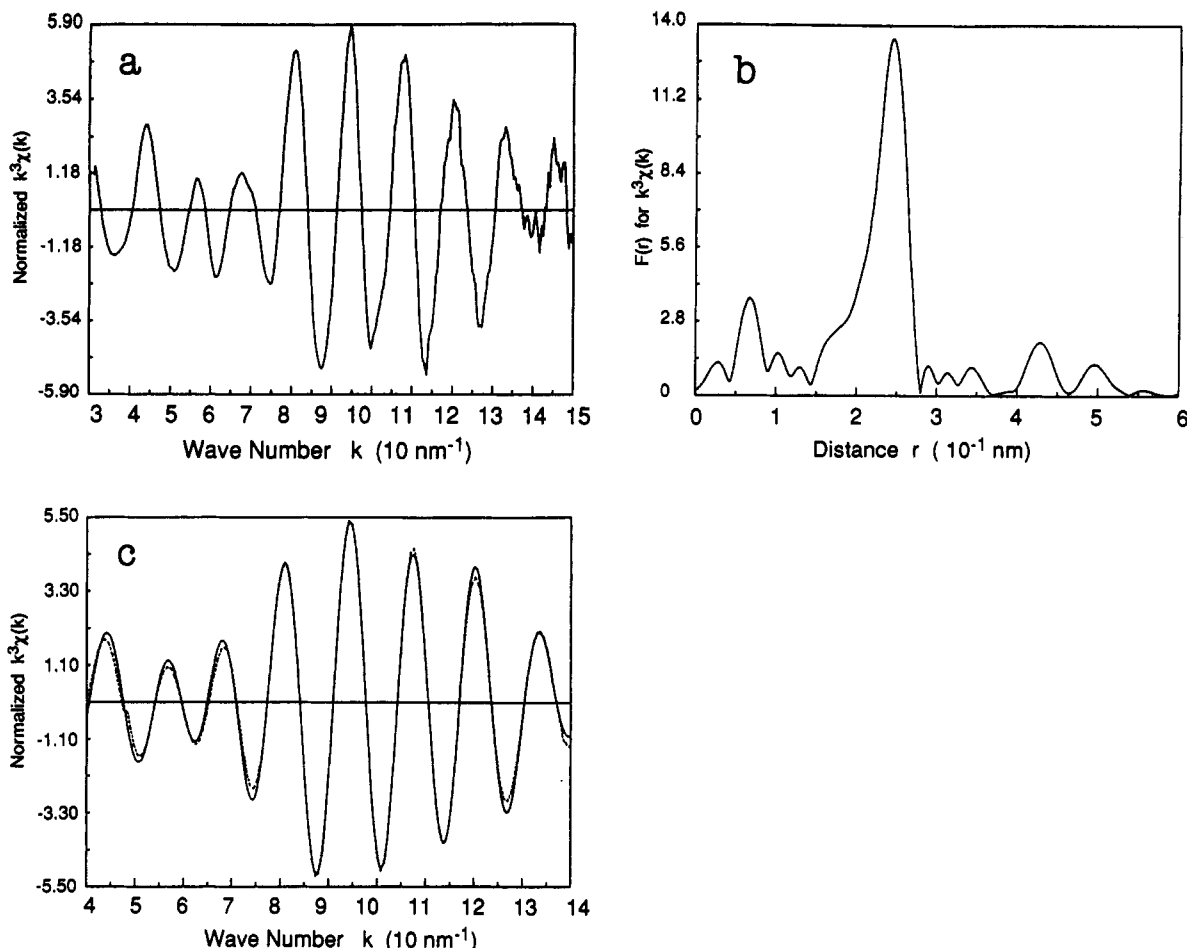
Figure 3. EXAFS spectra for Rh K-edge of Se-undoped Rh$_6$/MgO treated at 298 K: (a) k^3-weighted EXAFS oscillation, (b) its associated Fourier transform, and (c) inversely Fourier transformed curve-fitting analysis (—, observed; --, calculated).

Figures 7 and 8 and Table IV. For Rh$_6$/MgO the wavenumber and intensity of each peak were almost the same as those before hydroformylation. For the Se-doped catalyst (Figure 8b) the growth of two peaks at 2094 and 2022 cm^{-1} in ethene hydroformylation was observed (Table IV). We tried to find some correlation of these two peaks with ethene hydroformylation by using ^{13}CO, but the faster exchange of CO ligands with gas-phase ^{13}CO than the rate of ethene hydroformylation prevented us from further experiment under reaction conditions.

Discussion

Rh$_6$(CO)$_{16}$ reacted with MgO surface to form Rh$_6$(CO)$_{16-l}$/MgO (incipient cluster b in Scheme I), releasing about one (1–1.5) CO ligand per Rh$_6$, as proved by the analysis of CO evolved during the TPD spectrum and the amount of CO$_2$ formed in the oxidation of the TPD-treated species with O$_2$. The incipient Rh$_6$ carbonyl cluster was further decarbonylated to form the species Rh$_6$-(CO)$_{16-m}$ (c) in Scheme I by evacuation at 398 K, where m was about 6.5 by the analysis of CO evolved. The intensity of the IR peaks of the CO ligands in Figure 7 also suggests the loss of about one-third of the CO ligands in cluster c, which is compatible with the TPD data. Both terminal and bridged CO ligands were reduced in intensity. These ligands are exchangeable with each other at 398 K. When the partially-decarbonylated Rh$_6$(CO)$_{16-m}$ (c) on MgO was quantitively interacted with (CH$_3$)$_2$Se (1:1 stoichiometry) at 398 K, about one CO was evolved. Besides, the formate peaks at 1632, 1524, and 1388 cm^{-1} were observed by IR; the formates are formed by the reaction of CO with surface OH groups of MgO. The amount of the surface formates was estimated to be 1 molecule per Rh$_6$, judging from the peak intensity. Thus, the composition of the Se-doped Rh$_6$ cluster d on MgO is suggested to be [SeRh$_6$(CO)$_8$]/MgO, where one CO ligand was replaced by a Se atom and another CO ligand was desorbed at 398 K.

We examined the active structure of SeRh$_6$/MgO by means of EXAFS and IR. The coordination numbers of Rh–Rh for the incipient supported cluster b and the 398 K-treated cluster c were 3.8, as shown in Table II, which is close to the expected value (4) for the original cluster, suggesting that the Rh$_6$ framework was retained on the MgO surface. The Rh–Rh coordination number was not changed after the reaction with (CH$_3$)$_2$Se at 398 K, where it was 3.7 (species d) or 4.0 (species e), as shown in Table II. This demonstrates that (CH$_3$)$_2$Se reacted with cluster c without destroying the six rhodium atom cluster framework. The Rh–Rh bond distance is almost the same as samples a–d. The direct bonding of Se–Rh was observed at 0.244 nm with the sample of Se/Rh$_6$ = 1.0. For the sample of Se/Rh$_6$ = 2.0 the bond distances of Rh–Rh and Se–Rh decreased to 0.273 and 0.243 nm, respectively. The cluster framework may have shrank a little by the addition of two Se atoms to the Rh$_6$ framework.

The typical μ_3-CO peak around 1800 cm^{-1} for the Rh$_6$ carbonyl cluster was always observed in the range of $0 \leq$ Se/Rh$_6 \leq 2$ (Figures 7 and 8), which also confirms the retention of the Rh$_6$ framework.

The binding energy of Se 3d$_{5/2}$ for the catalyst with Se/Rh$_6$ = 1.0 was 54.7 eV. The value ranges between 53.5 eV for Se^{2-} (ZnSe and PbSe) and 55.9 eV for Se^0 (Se metal).[11] The XPS data revealed that the Se atom bonded to the Rh$_6$ cluster is negatively charged, possibly to be Se^{n-} ($n \simeq 1$). The binding energies of Rh 3d$_{5/2}$ and 3d$_{3/2}$ for Se/Rh$_6$/MgO were 307.1 and 311.7 eV, respectively, which correspond to those for Rh^0 species. Se is a more electronegative atom than Rh. If the positive charge induced by Se attachment is distributed over the cluster framework, the slightly charged Rh could not be discriminated from the Rh metallic state by XPS.[12]

Sulfur and selenium are preferably located at the μ_3 site in chalcogen-coordinated metal clusters,[13] though our results of EXAFS in Tables I and II cannot tell the exact value of the
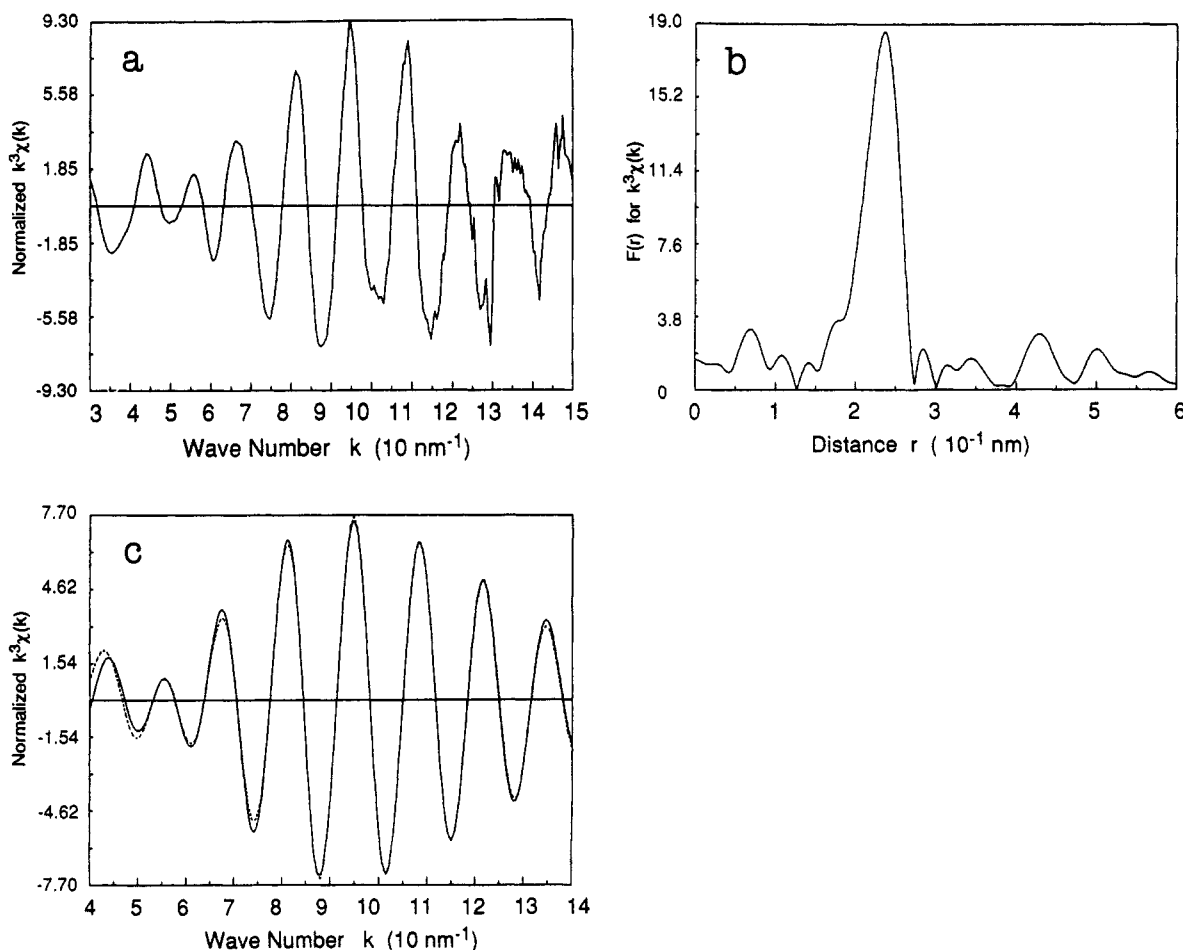
Figure 4. EXAFS spectra for Rh K-edge of Se-doped Rh_6/MgO (Se/Rh_6 = 2.0): (a) k^3-weighted EXAFS oscillation, (b) its associated Fourier transform, and (c) inversely Fourier transformed curve-fitting analysis (—, observed; - -, calculated).
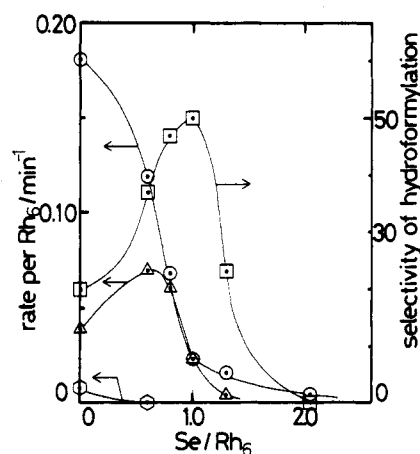

Figure 5. Catalytic activities and selectivities of ethene hydroformylation on the Se-doped Rh_6/MgO as a function of Se content: reaction temperature, 398 K; total pressure, 40.0 kPa; C_2H_4:CO:H_2 = 1:1:1; Rh, 1.3 wt %. Key: ⊙, ethane; ▲, propanal; ⊙, propanol.

Figure 6. CO uptake for Se-doped Rh_6/MgO (CO: 12 kPa, 298 K) and total amount of CO (CO uptake + ligand CO).

coordination number of Se–Rh because of the lack of an appropriate model compound with the Se–Rh bond. There are some Rh complexes or clusters with the coordination of Se, but the bond length of Se–Rh and the electronic state are too different from those for our Se-deposited catalysts and cannot be used as model compounds in the curve-fitting procedure. The coordination number of Se–Rh remained unchanged after the hydroformylation, which suggests the stable structure with μ_3-Se on the Rh_6 framework. The intensity of the peaks of the μ_3-CO ligands and the terminal CO ligands of the Rh_6 carbonyl cluster decreased by the interaction with MgO and the reaction with $(CH_3)_2$Se at 398 K in Figures 7 and 8. We propose supported structures for

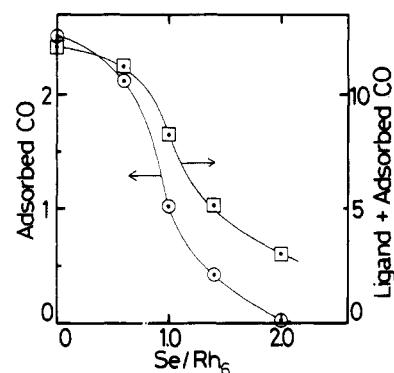the Se-undoped and -doped Rh_6 cluster in the CO atmosphere in Figure 9. These structures are based on (1) the retention of the cluster framework shown by the detailed EXAFS analysis, (2) the number of CO ligands on the Rh_6 unit in the samples after the interaction of the incipient Rh_6 cluster b with MgO surface at 398 K and after the reaction of species c (Scheme I) with $(CH_3)_2$Se, (3) the amount of CO uptake on species c and d (Scheme I) at 298 K, (4) the decrease in the intensity of the terminal and triply-bridged CO peaks by the treatments, and (5) the preferable location of Se atom at the μ_3 site. It is suggested by FT-IR that the face with the μ_3-CO preferentially interacts with the MgO surface at 398 K, releasing one μ_3-CO and five or six (due to heterogeneous environment of the surface) terminal CO's. When thus obtained partially-decarbonylated Rh_6 cluster c was exposed to CO at 298 K, two or three (average value: 2.5, as shown in Figure 6) CO molecules, corresponding to the case of the five or six terminal carbonyls removed, respectively, adsorbed
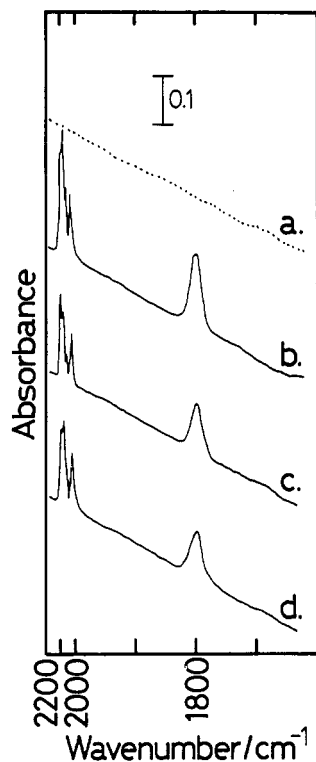
Figure 7. FT-IR spectra for Rh$_6$/MgO catalyst: (a) MgO, (b) incipient Rh$_6$/MgO, (c) sample evacuated at 398 K, and (d) sample after ethene hydroformylation for 60 min.
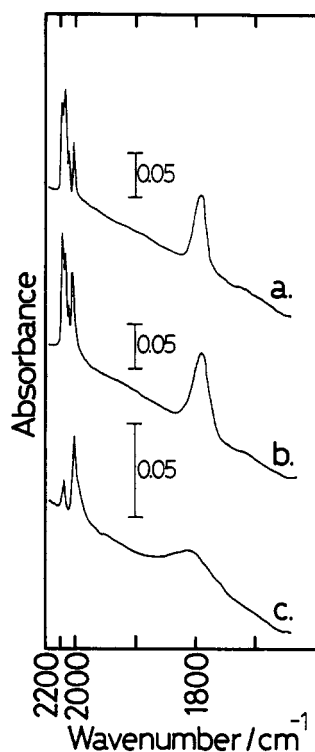

Figure 8. FT-IR spectra for Se/Rh$_6$/MgO catalysts (Se/Rh$_6$ = 1.0 (a, b) and 2.0 (c)): (a) after reaction with (CH$_3$)$_2$Se for 30 min at 398 K, (b) condition a after ethene hydroformylation for 60 min, and (c) after reaction with (CH$_3$)$_2$Se for 30 min at 398 K.

to recover half the twin carbonyls at the corners of the face interacted with the surface, as illustrated in Figure 9. Upon reaction with (CH$_3$)$_2$Se at 398 K, ca. three CO ligands were evolved as shown by the gas-phase analysis and the amount of formate, which corresponds to the decarbonylation of one μ_3-CO and two terminal CO ligands, as shown in Figures 7 and 8, accompanied with the formation of the Se–Rh bond at 0.244 nm in Table I and Figure 2. When the Se-modified Rh$_6$ cluster d was exposed to CO at 298 K, one CO adsorbed, as shown in Figure
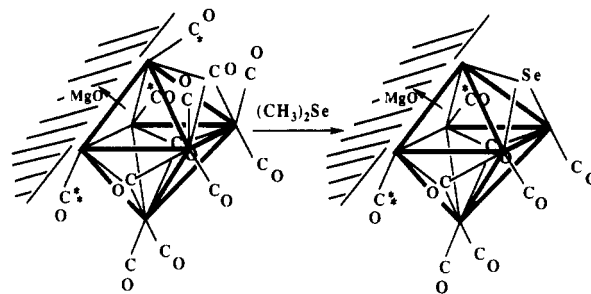

Figure 9. Proposed structures for Rh$_6$(CO)$_{12}$ and SeRh$_6$(CO)$_8$ (Se/Rh$_6$ = 1.0) clusters on MgO in CO atmosphere; *, removed at 398 K in vacuum; **, partially removed at 398 K in vacuum. The arrows imply the interaction of the face with MgO surface.

6, to form [SeRh$_6$(CO)$_8$] on MgO, as illustrated in Figure 9. The comprehensive data of FT-IR, EXAFS, and composition analysis demonstrate the structures in Figure 9 for the Rh$_6$ clusters supported on MgO. If the face of the cluster without the μ_3-CO was attached to the MgO surface, all of the experimental results could not be explained.

In the octahedral Rh$_6$ structure with μ_3 coordination of Se (Se/Rh$_6$ = 1.0) in Figure 9, three Rh atoms are directly bonded to Se, which correspond to the nearest-neighbor sites (Rh$_A$) in the Se/Rh(111) system, and the other three Rh atoms may correspond to the next-nearest-neighbor sites (Rh$_B$). In Figure 5 the selectivity of propanal formation increased by Se doping and showed a maximum at Se/Rh$_6 \simeq$ 1.0.

It is suggested that ethene hydrogenation needs more sites ($\geq$3) than ethene hydroformylation.[14,15] The selective site blocking by Se atom may be a reason for the increase of the selectivity to propanal. But the prominent increase of the catalytic hydroformylation rate per total Rh atoms by the Se addition in Figure 5 indicates the creation of a new active site for propanal formation. It has been demonstrated that the next-nearest-neighbor site (Rh$_B$) is an active site for the promotion of hydroformylation reaction in the Rh/ZrO$_2$ and Rh/SiO$_2$ catalysts.[6,7] The Rh$_B$ corner site of the SeRh$_6$ cluster in Figure 9 may be suggested to be the active site. When another Se atom was coordinated to the remaining μ_3 site of the Se-modified Rh$_6$ cluster, furthermore, the activity of the hydroformylation disappeared, as shown in Figure 5. This fact suggests that the Rh$_B$ site in the cluster is the active site for the hydroformylation. In the Rh/ZrO$_2$ and Rh/SiO$_2$ catalysts the selectivity and turnover frequency (TOF) (rate per surface unblocked Rh) increased by Se, but the reaction rate per total Rh did not increase. The promotion of catalytic hydroformylation on a supported Rh catalyst by S addition has been reported,[16] where S atoms were assumed to adsorb on the μ_3 site of the flat Rh(111) plane, without blocking of step sites. On Ru(1,1,10) single crystal S atoms at first selectively adsorb on the step sites, followed by the adsorption on the flat plane after the completion of the step site adsorption.[17]

The Rh$_A$ sites of the Se-modified Rh$_6$ cluster in Figure 9 should be most electronically effected by Se. Alternative explanation of the promotion of hydroformylation by the Se addition may be the creation of the Rh$_A$ sites as active sites. This possibility cannot be excluded at the present.

The selective structure for propanal formation is proposed to be the structure in Figure 9. However, the maximum reaction rate was observed at Se/Rh$_6 \simeq$ 0.6 in Figure 5, where a part of the Rh$_6$ clusters are not modified by Se. The reason for the different optimum Se content between the rate and the selectivity in the cluster system is not completely clear, but hydrogen spillover might occur from the Se-undoped cluster to the Se-doped cluster on MgO surfaces.

Conclusion

(1) The Se-doped Rh$_6$ cluster catalysts were prepared by the controlled reaction between the partially-decarbonylated Rh$_6$-(CO)$_{16-m}$ ($m \simeq$ 6.5) on MgO and (CH$_3$)$_2$Se at 398 K.

(2) Selenium increased the reaction rate for propanal formation in catalytic ethene hydroformylation.

(3) The selectivity of hydroformylation increased from 20 to 50%.

(4) Selenium was selectively bound to Rh at the bond distance of 0.243–0.244 nm by Se K-edge EXAFS.

(5) The Rh_6 cluster framework was maintained after the reaction with $(CH_3)_2Se$ as suggested by the coordination number of Rh–Rh in the Rh K-edge EXAFS and the peak at 1800 cm^{-1} for the μ_3-CO ligands.

(6) XPS showed that selenium on the Rh_6 cluster was situated in an oxidation state of ca. −1, while no shift of Rh 3d binding energies from the metallic level was observed.

(7) The structures of the partially-decarbonylated Rh_6 cluster and the Se-modified Rh_6 cluster on MgO were proposed on the basis of the number of CO ligands, its change by the treatments, FT-IR, and EXAFS.

(8) The active sites for the catalytic hydroformylation reaction were suggested to be Rh_A or Rh_B on the Rh_6 framework.

References and Notes

(1) (a) Gates, B. C., Guczi, L., Knözinger, H., Eds. *Metal Cluster in Catalysis*; Elsevier: Amsterdam, 1986. (b) Iwasawa, Y., Ed. *Tailored Metal Catalysts*; Reidel: Dordrecht, The Netherlands, 1986.

(2) Kirlin, P. S.; Knözinger, H.; Gates, B. C. *J. Phys. Chem.* **1990**, *94*, 8451.

(3) Lee, G.; Ponec, V. *Catal. Rev.—Sci. Eng.* **1987**, *29*, 183.

(4) Jackson, S. D.; Brandreth, B. J.; Winstanley, D. *J. Catal.* **1991**, *129*, 540.

(5) Chuang, S. S.; Pien, S. I.; Sze, C. *J. Catal.* **1990**, *126*, 187.

(6) Izumi, Y.; Asakura, K.; Iwasawa, Y. *J. Catal.* **1991**, *127*, 631.

(7) Izumi, Y.; Asakura, K.; Iwasawa, Y. *J. Catal.* **1991**, *132*, 566.

(8) MacLaren, J. M.; Pendry, J. B.; Joyner, R. W. *Surf. Sci.* **1986**, *178*, 856.

(9) Teo, B. K. *EXAFS: Basic Principles and Data Analysis*; Springer: Berlin, 1986.

(10) Chini, P. *J. Chem. Soc., Chem. Commun.* **1967**, 440.

(11) Ley, L.; Pollak, R. A.; McFeely, F. R.; Kowalczyk, S. P.; Shirley, D. A. *Phys. Rev. B* **1974**, *9*, 600.

(12) Baltanas, M. A.; Onuferko, J. H.; McMillan, S. T.; Katzer, J. R. *J. Phys. Chem.* **1987**, *91*, 3772.

(13) Galli, D.; Garlaschelli, L.; Ciani, G.; Fumagalli, A.; Martinengo, S.; Sironi, A. *J. Chem. Soc., Dalton Trans.* **1984**, 55.

(14) Sachtler, W. M. H. *Faraday Discuss. Chem. Soc.* **1981**, *72*, 7.

(15) Siegel, S. *J. Catal.* **1973**, *30*, 139.

(16) Konishi, Y.; Ichikawa, M.; Sachtler, W. M. H. *J. Phys. Chem.* **1987**, *91*, 6186.

(17) Egawa, C.; Iwasawa, Y. *Surf. Sci.* **1988**, *198*, L329.

Ellipsometric Study of Surfactants Comprising Linear and Branched Hydrocarbon Chains at the Air–Water Interface

L. Ghaïcha, R. M. Leblanc,

Centre de Recherche en Photobiophysique, Université du Québec à Trois Rivières, CP.500 Trois Rivières, Québec G9A 5H7, Canada

and A. K. Chattopadhyay*

ICI Explosives Group Technical Centre, McMasterville Site, 801 Richelieu Blvd., McMasterville, Quebec J3G 1T9, Canada (Received: June 23, 1992; In Final Form: September 14, 1992)

The ellipsometric isotherms of diethanolamine derivatives of *n*-alkylsuccinic anhydride (where the alkyl group comprised C12, C14, and C16 hydrocarbon chains) and polyisobutylene succinic anhydride (where the average backbone carbon numbers of polyisobutylene chains were 14, 22, and 34) at the air–water interface were compared with a view to the development of an understanding of the structural organisation of their monomolecular films. The ellipsometric angle, $\Delta\delta$, has proven to be very sensitive to the nature of the physical state of the film that occurs during film compression. At 20 ± 1 °C, the two series of surfactants exhibited very different behavior upon compression. A rodlike model was used to describe the different molecular behaviors exhibited by the surfactants comprising linear and branched hydrocarbon chains. Equations relating variations of refractive indexes, film thicknesses, and molecular areas were used for the determination of the molecular properties of the films during monolayer compression. Calculated refractive indexes and film thicknesses were obtained from experimental $\delta\Delta$ values. The results indicated that the change in $\delta\Delta$ values during film compression is more sensitive to the refractive indexes than to the film thicknesses. For the surfactants with *n*-alkyl chains the refractive index component increased linearly, whereas a reverse trend was observed with the surfactant molecules comprising polyisobutylene chains. Such an anomaly in refractive index can be explained by the effect of substituents in the hydrocarbon chains and subsequent differences in packing behavior of monolayers. The $|\delta\Delta|$ of *n*-alkyl derivatives increased upon compression and reached a steady state at collapse pressure, whereas a sharper rise in $|\delta\Delta|$ was observed with the derivatives comprising polyisobutylene chains. Such phenomena indicated multilayer formation by the molecules with polyisobutylene chains in the collapse region.

Introduction

The role of molecular structure, polar head-group charge, and the influence of counterions on the polar head groups of surfactants has great significance in determining their interfacial properties.[1-6] These phenomena have been studied in detail in the past with little attention having been paid to the nonpolar components of surfactants.

However, more recently, attention has been turned toward the nonpolar group of the amphiphilic molecules.[7,8] Biologists, for instance, are interested in the components of surfactant molecules which possess unsaturation or substitution in their hydrophobic region. It has been found that in some membranes fatty acids possess unsaturation or substitution in their hydrophobic chains.[9]

The properties of such fatty acids adsorbed at the interface in biological membranes are dependent partly on the lateral interactions between adjacent alkyl chains. This leads to greater fluidity and permeability of surface films in membranes composed of such fatty acids.

The behavior of certain fatty acids and lecithin has been studied at the air–water interface by surface pressure–area measurements. It was reported that the unsaturated or branched hydrocarbon chains of such molecules lead to an expansion of their molecular area when compared to the corresponding saturated or unsubstituted molecules.[8,10-13]

* To whom correspondence should be addressed.